Journal of Neuroscience Methods 177 (2009) 334–347

Contents lists available at ScienceDirect

Journal of Neuroscience Methods

journal homepage: www.elsevier.com/locate/jneumeth

Optimal spectral tracking—With application to speed dependent neural modulation of tibialis anterior during human treadmill walking

John-Stuart Brittain[a,*], Celia Catton[b], Bernard A. Conway[b], Jens Bo Nielsen[c,d], Ned Jenkinson[e], David M. Halliday[a]

[a] Department of Electronics, University of York, York YO10 5DD, UK
[b] Biomedical Engineering Unit, University of Strathclyde, Glasgow, UK
[c] Division of Neurophysiology, Department of Medical Physiology, The Panum Institute, University of Copenhagen, Denmark
[d] Department of Exercise and Sport Sciences, University of Copenhagen, Denmark
[e] Nuffield Department of Surgery, Oxford University, Oxford, UK

ARTICLE INFO

Article history:
Received 25 June 2008
Received in revised form 13 October 2008
Accepted 15 October 2008

Keywords:
Spectral tracking
Locomotion
Gait
Coherence
Adaptive-filtering
Tibialis anterior

ABSTRACT

A novel method of optimal spectral tracking is presented which permits the characterisation of trial-varying parameters. Many experimental studies suffer from the limitations of available analysis methodologies, which often impose a condition of stationarity. This severely limits our ability to track slow varying or dynamic responses with any statistical certainty. Presented is a complete framework for the non-stationary analysis of trial-varying data. Theory is introduced and developed in the characterisation of speed dependent neural modulation of the locomotor drive to tibialis anterior (TA) during healthy treadmill locomotion. The approach adopts adaptive filter theory while retaining a spectral focus, thus remaining compatible with much of the current literature. Spectral tracking procedures are evaluated using both surrogate and neurophysiological time-series. Confidence intervals are derived in both empiric and numerical form. Analysis of the pre-synaptic drive to TA under the modulation of treadmill belt speed follows, with results demonstrating clear speed dependent influences on the spectral content of TA, suggesting dynamic neural modulation of the locomotor drive. Findings include speed-modulated components at 7–12 Hz (early swing) and 15–20 Hz (pre-stance). Speed invariant components were identified at 8–15 and 15–20 Hz during early and late swing, in agreement with previous studies. Modification to the method permits a sub-optimal alternative, encouraging the exploration of short epoched data.

1. Introduction

Speed dependent neural modulation of the central pattern generating (CPG) rhythm in humans remains a relatively unexplored area of gait research. Though the modulatory effects of locomotor speed on EMG profiles have long been ascertained (Murray et al., 1984), research into their neural origins remain elusive. Such research could provide key insight into the functional organisation of CPG systems alongside the influence of descending supra-spinal pathways.

A fundamental method of exploring modulation is to adjust some control parameter and observe the consequences. Many neurological studies concerned with frequency domain statistics however require a 'repeat-trials' philosophy. This approach is necessitated by the requirements of available analysis techniques, which often impose the condition of wide-sense stationarity (Halliday et al., 1995)—that the second order moments between signals x_n and y_n, given by $E\{x_n y_{n+\tau}\}$, are themselves independent of n. This restriction severely limits our ability to track parameter changes during dynamic, non-repetitive actions. Where trials may be ordered such that neighbouring epochs are considered statistically similar, this information should be exploited to produce an estimate of trial-relative spectra. A naive approach to the problem could involve application of a simple moving-average or exponential decay function over trials in which distributional information is ignored.

What follows is the presentation of a novel method for optimal spectral tracking which permits the characterisation of trial-varying parameters while facilitating the construction of multivariate statistics such as phase and coherence. Application is made to surrogate and neurophysiological data, with a focus on the changing pre-synaptic drive to tibialis anterior (TA) during speed-modulated treadmill locomotion in healthy volunteers. The

* Corresponding author. Tel.: +44 1904 432345; fax: +44 1904 432335.
E-mail addresses: jsb122@ohm.york.ox.ac.uk, john-stuart.brittain@dpag.ox.ac.uk (J.-S. Brittain).

0165-0270/$ – see front matter © 2008 Elsevier B.V. All rights reserved.
doi:10.1016/j.jneumeth.2008.10.028

framework provides sufficient generality to be applicable to a wide range of locomotor and non-locomotor based protocols.

Tracking procedures may be augmented with optimal spectral smoothing techniques to provide point estimates conditioned on the entire observation sequence. Confidence limits are placed and the method reviewed in a comparative study with potential future applications outlined. The optimality framework imposes distributional assumptions on the spectra of individual trial epochs. Should these assumptions fail, an alternative sub-optimal solution is posed which utilises a zero-skew transformation of the spectral statistics.

It is hoped that the ability to quantify trial-varying parameters will encourage the development of more complex experimental protocols, permitting more expansive investigations into the neural response to dynamic actions. The framework is amenable to numerous potential applications including studies of arousal, heart-rate variability, sleep stage classification, fatigue, epilepsy, anaesthetic monitoring and drug response.

2. Materials and methods

In preparation of the optimal spectral tracking framework, it is necessary to outline the required preprocessing procedures. Appropriate segmentation of the data is first discussed in conjunction with normalisation strategies for both epoched and single-trial time series. In the case of epoched data, the mean excitation envelope often provides the most appropriate measure for final epoch selection. This approach can often be confounded however, where data display trial-varying non-stationarity, manifest as inconsistent epoch lengths. To address this restriction, a new measure of envelope modulation is introduced which explicitly accounts for variations in trial length. This measure is dubbed the Normalised Activity Envelope (NAE). Following segmentation, spectral measures are obtained where both their native and transformed distributions are discussed. The spectral estimators then undergo tracking through data-adaptive filtering procedures. Augmentations to the spectral tracking approach are discussed, which include adaptive spectral smoothing and an alternative zero-skew symmetric transformation. Aspects of statistical inference such as bandwidth and the placement of confidence limits are also discussed.

2.1. Segmentation strategy

The spectral analysis of time-series often involves consideration of data as either a sequence of trials, identified through an associated set of triggers, or as single-trial data split into equal length segments. For data where the interval of interest is defined by a set of M triggers, the duration of activity may not always be consistent. For single-trial data, the record may be decomposed into M disjoint sections of equal length N samples. As a generalisation, 'segment' will refer to either a trial identified from a set of triggered epochs or a section of data obtained through disjoint segmentation.

Optimal spectral tracking requires a set of spectral observations. The simplest single-segment estimator is the periodogram, though alternative methods such as multitaper spectral estimates (see Thomson, 1982) are equally valid. The periodogram, or multitaper estimate, for a time-series x at segment m will be denoted $P_{xx}^{(m)}(f)$, evaluated at the Fourier frequencies $f_n = n/(N\Delta t)$ for $n = 0, \ldots, \lfloor N/2 \rfloor$ with Δt the sampling interval. To obtain alignment at the Fourier frequencies, data segments are zero padded to a common length N samples prior to processing.

It will become necessary to distinguish between single-segment spectral estimates and processed spectra derived through optimal tracking procedures. The single-segment cross-spectral estimate between processes x and y for frequency f at segment m will be denoted $P_{xy}^{(m)}(f)$. The elusive underlying spectrum will be denoted $S_{xy}^{(m)}(f)$, with $\hat{S}_{xy}^{(m)}(f)$ the estimate derived through optimal filtering or smoothing procedures.

Within the current framework it is assumed that individual segments represent regions of co-activity, i.e. for bivariate data, that segment m of channel 1 occurs over the same time interval as segment m of channel 2. It is further assumed that estimates of the spectra for segment m are obtained using identical analysis parameters across channels.

Since the primary statistic of interest here is the power spectrum, it is intuitive to power normalise segments prior to analysis, thus providing a relative measure of power change in each frequency band across segments. Power normalisation is accomplished for real-valued data at each trial m by

$$\tilde{x}_n^{(m)} = \frac{x_n^{(m)}}{\sqrt{\frac{1}{N_m}\sum_{k=0}^{N_m-1}\left(x_k^{(m)}\right)^2}} \tag{1}$$

where $x_n^{(m)}$ represents the data sequence for trial m of length N_m samples (prior to zero padding) with $\tilde{x}_n^{(m)}$ its power normalised equivalent.

Where trigger times for a series of epochs do not directly correspond to the period of interest (e.g. lower limb muscle activity in relation to heel contact with a treadmill belt), a measure of envelope modulation is required. Where data display consistent trial lengths, the Spike-Triggered Average (STA) (Halliday et al., 1995, 1998) may be considered an appropriate measure of envelope modulation. For variable duration data however, the STA is inappropriate as it does not consider inherent trial-to-trial variations in epoch length. To address this issue a population measure is introduced which permits identification of relative common activity across variable duration trials—the NAE.

2.2. Normalised Activity Envelope

In calculating activity envelopes, we take a frequency domain approach in keeping with the current framework. Each trial m of length N_m, for $m = 1, \ldots, M$, is Fourier transformed and subsequently zero padding to N samples in the frequency domain. Frequency domain zero padding occurs at the mid-point and not the end of the series as is the case in the time-domain. The resulting interpolated time-series $\mathring{x}_{n'}$ is recovered by taking the N sample inverse Fourier transform. Each trial is mean subtracted and power normalised prior to Fourier transformation in an effort to maintain equal weighting between dissimilar length epochs, and also in anticipation of confidence limit construction. Taking $X_n = \mathcal{F}\{x\}$ as the Fourier transform of x_n for $n = 0, \ldots, N_m - 1$ and $\mathcal{F}^{-1}\{\bullet\}$ the inverse Fourier transform, the interpolation procedure may be described by

$$\mathring{x}_{n'} = \sqrt{\frac{N}{N_m}}\mathcal{F}^{-1}\left\{X_0, \ldots, X_{\lfloor N_m/2 \rfloor}, \underbrace{0, \ldots, 0}_{(N-N_m)\,\text{zeros}}, X_{\lfloor N_m/2+1 \rfloor}, \ldots, X_{N_m-1}\right\}. \tag{2}$$

If the zeros are added correctly then the inverse Fourier transform should result in a real-valued time-series. In maintaining unit power a corrective factor $\sqrt{N/N_m}$ is applied to the duration-normalised trials. The resulting set of time-series are all of equal length N samples, where n' (for $n' = 0, \ldots, N-1$) corresponds to a relative position within the normalised time-base. Taking the mean of these duration normalised trials provides an appropriate envelope for feature extraction. It is suggested, especially in electromyogram (EMG) recordings where a zero mean process is

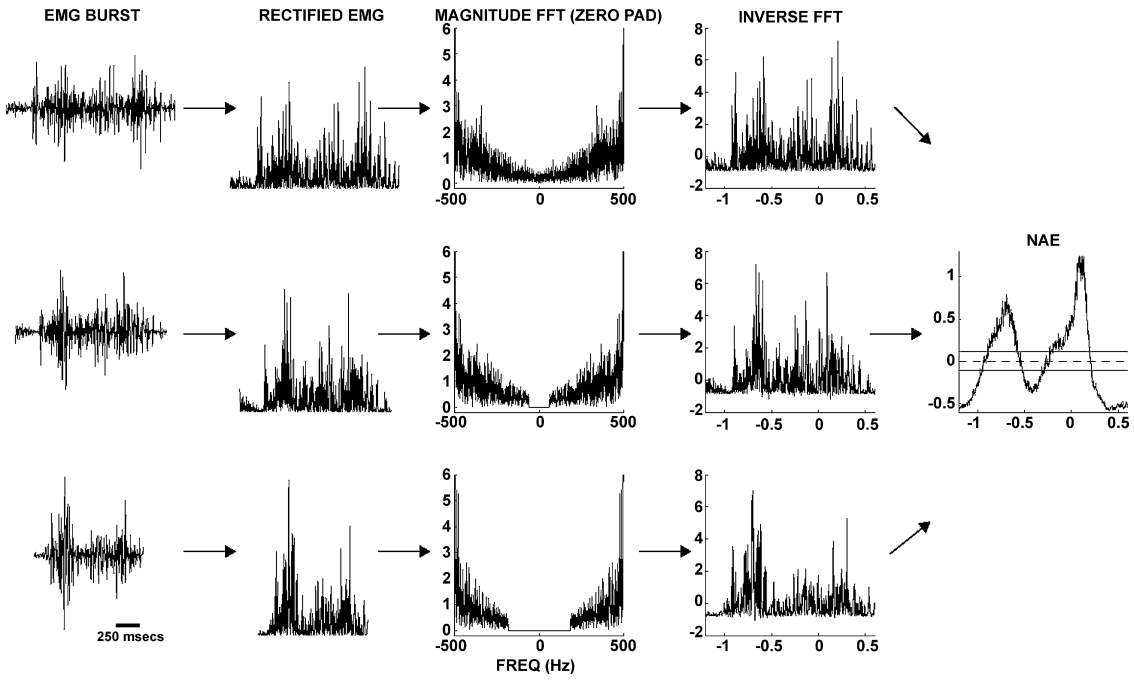

Fig. 1. Illustration of the NAE construction process. Displayed are three bursts of TA EMG activity from the variable speed treadmill locomotion dataset. Decreased stride length with increasing belt speed leads to a shortening of EMG burst duration (top-to-bottom). EMG data are full-wave rectified (to elucidate envelope modulation), then Fourier transformed where frequency domain zero padding is applied. Data are subsequently inverse Fourier transformed and averaged to produce a group measure of envelope modulation on a normalised time-base—the NAE. The final NAE displayed corresponds to averaging over 176 trials.

assumed, to full-wave rectify data segments prior to NAE construction to emphasis the time-course of muscle activation. An illustration of the NAE construction process for the variable speed locomotion dataset (to be discussed) is presented schematically in Fig. 1.

Significance limits for NAEs may be placed under the null hypothesis of independence by considering the construction process. Recall that each trial is mean subtracted and power normalised prior to Fourier transformation. This ensures the sample variance of each trial is 1, maintained throughout the padding procedure by the corrective factor $\sqrt{N/N_m}$. The resultant series of equal length trials are then averaged to produce an NAE. Since the sequence of trials may be considered a finite number of M independent, identically distributed (i.i.d.) random variables of unit variance, the variance of the sum is simply M. This follows from a special case of Wald's theorem, in which a sequence of i.i.d. random variables $X = \{X_1, \ldots, X_M\}$ are defined with non-negative integer value M independent of X. The mean of the sum of sequence elements is given by $\mathrm{E}\{M\}\mathrm{E}\{X\}$, with variance $\mathrm{E}\{X\}^2\mathrm{var}\{M\} + \mathrm{E}\{M\}\mathrm{var}\{X\}$ (Drake, 1967). In considering the mean and not simply the sum, a scaling factor $1/M$ must be applied. The sum is assumed Gaussian under the central limit theorem, thus the variance becomes the variance of the sum times the square of the scaling factor, i.e. $M(1/M)^2 = 1/M$ (Drake, 1967). The NAE distribution for the case of independent trials may therefore be considered approximately Gaussian with variance $1/M$. Confidence limits may be placed about the origin which, at the 95% level, are given by $0 \pm 1.96/\sqrt{M}$.

2.3. Transform filtering

The statistical properties of power spectra are well documented in both frequency and log domains (Brillinger, 1981; Percival and Walden, 1998; Bloomfield, 2000). A logarithmic transform will produce spectra approaching the normal distribution. Specifically, the spectral estimates will be distributed proportional to $\ln \chi^2_\nu$ (see Fig. 2). Consequently, though the log-periodogram ($\nu = 2$) remains markedly skewed, the normal approximation improves if multitaper methods are employed due to an increase in the number of degrees-of-freedom. In addition, multitaper methods produce more consistent single-segment estimators, though a degradation in frequency resolution is incurred. The optimal filtering solution for a series of estimators corrupted by Gaussian white noise is provided analytically by the Kalman filter. The Kalman filter provides a vector state estimation algorithm, optimal in the minimum mean-square error sense for additive process and measurement noise sources. The log-domain characteristics of spectral estimators are therefore briefly discussed before embedding said estimates into an optimal tracking framework through application of Kalman filtering techniques.

The proposed optimal tracking procedure requires normally distributed data for both auto- and cross-spectral measures. Frequency domain auto-spectra are, by construction, real-valued and positive, permitting direct transformation to the log-domain. The cross-spectrum however is complex-valued, where the real and imaginary parts are not restricted to the positive half-plane.

Taking the direct log-transform of the cross-spectra results in a disentanglement of the magnitude and local phase of the complex-vector $S^{(m)}_{xy} = |S^{(m)}_{xy}|e^{i\phi}$,

$$\ln S^{(m)}_{xy}(f) = \ln |S^{(m)}_{xy}(f)| + i\phi. \tag{3}$$

Such disentanglement is undesirable, leading to high levels of bias in the coherence estimate. It is important during the recursive optimal estimation procedure that the cross-spectra undergo an equivalent transformation to the auto-spectra. This is especially evident for measures such as coherence which produce bounded estimates. The real and imaginary parts of the cross-spectra are therefore separated before processing with the Kalman filter. Accordingly, $\ln \Re\{P^{(m)}_{xy}(f)\}$ and $\ln \Im\{P^{(m)}_{xy}(f)\}$ are evaluated prior to filtering. Both quantities will be complex-valued since we are

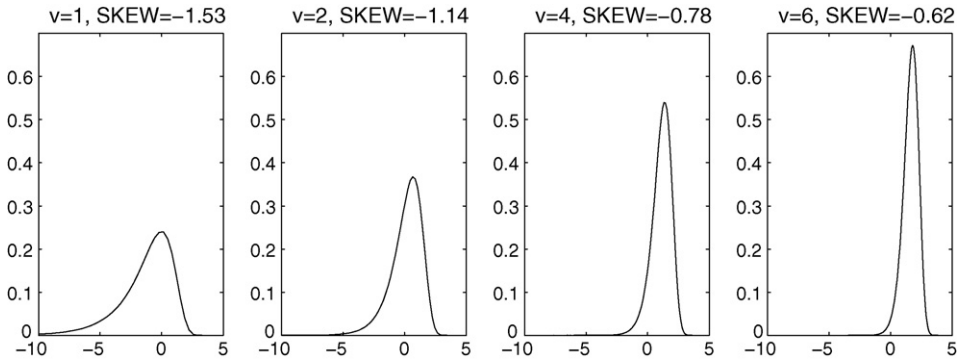

Fig. 2. Probability density functions for the natural logarithm of χ^2_ν random variates with $\nu = \{1, 2, 4, 6\}$ degrees of freedom.

taking the log of potentially negative values. Though processed separately, both are subject to the same matrix operations.

In order to recover the processed cross-spectra we take

$$S_{xy}^{(m)}(f) = \Re\left\{\exp\left(\mathcal{H}\left(\ln\Re\left\{P_{xy}^{(1,\ldots,m)}(f)\right\}\right)\right)\right\} + i\Re\left\{\exp\left(\mathcal{H}\left(\ln\mathcal{I}\left\{P_{xy}^{(1,\ldots,m)}(f)\right\}\right)\right)\right\} \quad (4)$$

where $\mathcal{H}$ represents a smoothing operator over the history of observations $P_{xy}^{(1,\ldots,m)}(f)$, in this case processing by a Kalman filter.

It is important at this point to consider the evaluation of $\ln(0)$, defined asymptotically as negative infinity. Spectral quantities close to zero may therefore lead to numerical instability within the tracking algorithm. The practical approach taken in this study is to place a lower bound on log-transform values of, say, -100. This corresponds to a frequency domain value of 3.7×10^{-44}.

The tracking procedure takes log-spectra as input measurements. The log-spectral variance is also required, given by Percival and Walden (1998)

$$\mathrm{var}\{\ln\hat{S}_{xx}^{(m)}(f)\} = \psi'(L) \quad (5)$$

for $0 < f < 1/(2\Delta t)$ with $\psi'(L)$ the trigamma function. L represents the number of segments making up the spectral estimate. When $f = \{0, 1/(2\Delta t)\}$ variance becomes $\psi'(L/2)$. For the periodogram $L = 1$. For multitaper methods L corresponds to the equivalent number of tapers utilised in the single-segment estimate (see Percival and Walden, 1998, 2000).

The Kalman filter, optimal for linear systems with additive Gaussian process and measurement noise, is utilised in the tracking of spectral components. In employing Kalman filter techniques, we equate input measurement vector $\mathbf{z}_k$ with single-segment estimators $P_{xy}^{(k)}(f)$ and state vector $\mathbf{x}_k$ with $\hat{S}_{xy}^{(k)}(f)$. We then attempt to track local changes in $\hat{S}_{xy}^{(k)}(f)$ based on our statistical knowledge of $P_{xy}^{(k)}(f)$. The Kalman filter operates over a state-space model, with state and measurement equations given by

$$\mathbf{x}_{k+1} = \varphi_k\mathbf{x}_k + \boldsymbol{w}_k$$
$$\mathbf{z}_k = \boldsymbol{H}_k\mathbf{x}_k + \mathbf{v}_k$$

where $\boldsymbol{w}_k$ and $\mathbf{v}_k$ are the process and measurement noise sources. Both are considered normally distributed with zero mean possessing covariance matrices $\mathbf{Q}$ and $\mathbf{R}_k$ respectively. We take process noise covariance $\mathbf{Q}$ to be a tracking parameter and therefore define it to be time invariant. Our state estimate is that of the underlying spectrum, thus the state-to-measurement matrix $\boldsymbol{H}_k$ is taken as the identity matrix $\mathbf{I}$. Similarly, since the filter will directly track the underlying spectrum, state-transition matrix φ_k is also chosen to be the identity matrix $\mathbf{I}$. While the state-transition matrix assumes a constant underlying spectrum, the estimate itself will be capable of tracking spectral changes through the inclusion of a non-zero additive process noise term.

The column vector $\mathbf{z}_k$, corresponding to single-segment estimators, is described by

$$\mathbf{z}_k = \left[\ln(P_{xx}^{(k)}(f_0)), \ldots, \ln(P_{xx}^{(k)}(f_{\lfloor N/2\rfloor})), \ln(P_{yy}^{(k)}(f_0)), \ldots, \ln(P_{yy}^{(k)}(f_{\lfloor N/2\rfloor})), \ln(\Re\{P_{xy}^{(k)}(f_0)\}), \ldots, \ln(\Re\{P_{xy}^{(k)}(f_{\lfloor N/2\rfloor})\}), \ln(\Im\{P_{xy}^{(k)}(f_0)\}), \ldots, \ln(\Im\{P_{xy}^{(k)}(f_{\lfloor N/2\rfloor})\})\right]^{\mathrm{T}}. \quad (6)$$

Column-vector $\mathbf{x}_k$ is similarly defined, substituting the conditioned spectral estimates $\hat{S}_{xy}^{(k)}(f)$ in-place of single-segment measurements $P_{xy}^{(k)}(f)$. The error-covariance matrix for measurement noise, $\mathbf{R}_k$, is a diagonal matrix containing the single-segment variances.

The Kalman filter algorithm is initialised by

$$\mathbf{x}_1 = \mathbf{z}_1, \quad \mathbf{P}_1 = \mathbf{R}_1$$
$$\mathbf{x}_2^p = \mathbf{x}_1, \quad \mathbf{P}_2^p = \mathbf{P}_1 + \mathbf{Q}$$

with $\mathbf{x}_1$ and $\mathbf{P}_1$ the *a posteriori* estimates of the state and error-covariance matrix at segment 1 and $\mathbf{x}_2^p$ and $\mathbf{P}_2^p$ the *a priori* state and error-covariance matrix for segment 2. Given the previously defined state-space model, Kalman tracking may be performed by the following update and projection equations for $k = 2, \ldots, M$ (See Brown and Hwang, 1997; Haykin, 2004 for more comprehensive coverage of Kalman filtering techniques).

Update
$$\mathbf{K}_k = \mathbf{P}_k^p(\mathbf{P}_k^p + \mathbf{R})^{-1}$$
$$\mathbf{x}_k = \mathbf{x}_k^p + \mathbf{K}_k(\mathbf{z}_k - \mathbf{x}_k^p)$$
$$\mathbf{P}_k = (\mathbf{I} - \mathbf{K}_k)\mathbf{P}_k^p$$

Projection
$$\mathbf{x}_{k+1}^p = \mathbf{x}_k$$
$$\mathbf{P}_{k+1}^p = \mathbf{P}_k + \mathbf{Q}$$

Filtering produces a series of M spectral estimates at the Fourier frequencies, each localised about their respective trial. The degree of localisation is dependent upon the choice of filter parameters (specifically $\mathbf{Q}$) leading to a fundamental trade-off between localisation and consistency. Localised estimates of auto- and cross-spectra are extracted directly as output from the filtering procedure. Localised estimates of bivariate parameters, such as phase and coherence (see Halliday et al., 1995), may be computed in pointwise fashion from their respective localised spectra.

Since we wish to estimate spectral ordinates independently, the covariance matrix passed to the Kalman filter remains strictly diagonal. Under this restriction the Kalman filter may be adapted to

a more efficient reduced vector implementation. This is accomplished by reducing matrices to vectors (taking the diagonal), discarding transpose operators and replacing ordinary matrix products with the (elemental) Hadamard product.

The Kalman filter may also be augmented by smoothing procedures, permitting filtered estimates of the spectrum to be conditioned on the entire measurement sequence. Various approaches exist to smoothing, though a simple solution is to perform filtering in the forward direction and then filter the forward output in a backwards direction. Kalman equations have been derived for this form of smoothing process which provide optimal estimates of the smoothed state vector and error-covariance matrix (Brown and Hwang, 1997).

In order to distinguish between filtered and smoothed states, the smoothed state vector and error-covariance matrix will be denoted $\tilde{\mathbf{x}}_k$ and $\tilde{\mathbf{P}}_k$ respectively. The smoothing algorithm is provided below for $k = M-1, \ldots, 1$. $\mathbf{A}_k$ is the backward gain matrix. A computationally efficient reduced-vector implementation may be derived in analogy with the tracking approach.

$$\mathbf{A}_k = \mathbf{P}_k(\mathbf{P}^p_{k+1})^{-1}$$
$$\tilde{\mathbf{x}}_k = \mathbf{x}_k + \mathbf{A}_k(\tilde{\mathbf{x}}_{k+1} - \mathbf{x}^p_{k+1})$$
$$\tilde{\mathbf{P}}_k = \mathbf{P}_k + \mathbf{A}_k(\tilde{\mathbf{P}}_{k+1} - \mathbf{P}^p_{k+1})\mathbf{A}^T_k$$

The bandwidth at each successive estimate can be determined through both filtered and smoothed approaches by considering the equivalent taper representation, in analogy with Thomson (1982). The equivalent data taper may be constructed as the weighted sum of data tapers applied to each segment (thus accounting for length variations), with weighting determined by the Kalman gain matrix. Since tapering is applied prior to zero padding, the padding procedure itself has no effect on equivalent taper bandwidth.

2.4. Pooling datasets

Data pooling may be accomplished through the concatenation of trial sequences prior to application of the spectral tracking routines. Tracking may be performed over either sorted or unsorted data, specific to the experimental hypothesis to be tested. For example, EMG activity recorded on an accelerating treadmill belt may be pooled across subjects in the construction of a summary dataset. If a criterion exists for trial ordering (treadmill speed in this case), then trials may be sorted prior to analysis. The result is an intermingled set of unit variance epochs from all subjects ordered by locomotor speed. For ordered data, tracking routines will only extract features common across subjects. Care must be taken to ensure an equivalent experimental protocol is performed for each subject however, else clustering of subject-specific trials may occur during the sorting procedure.

2.5. Time–frequency tracking

The premise of time–frequency tracking requires the sectioning of a single trial into multiple segments. Each segment is then tracked individually over the evolution of the experiment. The resulting spectra are then recombined into a time–frequency grid at each iteration of the analysis. Graphic illustration of the approach is provided in Fig. 3. Note that there is no restriction for the segment offset and width arguments to be uniform—indeed it is recommended that any segmentation be determined by visual examination of the data.

In consequence, the analysis framework has now been extended to provide three variables for spectral plotting—namely frequency, real-time (tracking across trials) and relative-time (segmentation within trials). This allows a wide choice of presentation methods

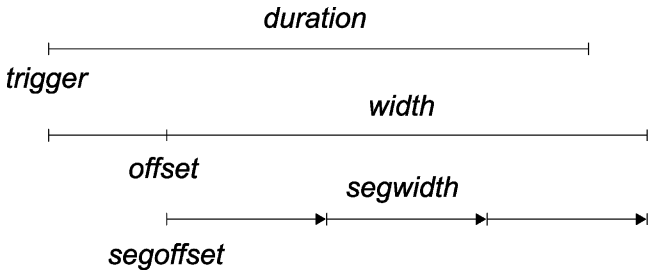

Fig. 3. Time-segmentation strategy for a single trial. Epoch split into $D = 3$ subsegments. In this example trigger points do not precisely match the region of interest. Parameters *offset* and *width* therefore provide alignment prior to segmentation.

to be considered. If we are interested in the behaviour of a single segment, we may plot real-time (across trials) versus frequency for that segment, where such analysis reduces to equivalent single-segment tracking. If we are interested in the evolutionary state of a specific trial, a more traditional time–frequency representation may be considered, with spectra made consistent through the inclusion of neighbouring trials in the estimate. For a specific frequency range of interest, figures may be produced highlighting frequency modulation in a real and relative time-dependent manner, i.e. real-time across trials versus relative-time within trials. Besides these representations, fixing two variables permits further consideration of the data.

2.6. Alternate transforms

The logarithm provides a variance stabilising transform for spectral estimates. It is not however the only applicable transform to adopt within the spectral tracking framework. The logarithm, while variance stabilising, does not provide a good symmetrical distribution, despite its asymptotic convergence to normality under averaging (see Fig. 2). This problem is especially pronounced for the periodogram where the logarithmic transform can produce significantly skewed distributions. It has been suggested that for a reasonable approximation to normality, log multitaper estimates using a time–bandwidth product of 10 or more are required (Percival and Walden, 2000). Such local smoothing would substantially reduce the interpretable frequency resolution of any subsequent analysis.

An alternative transform which has found prior application is the cube-root, described as producing a more symmetrical distribution (Thomson, 1982). The trade-off to this approach is that the variance is no longer stabilised, i.e. the variance expression required for use within the Kalman filter is dependent upon the unknown underlying spectrum.

In application of a more generalised rth-root transform, variance expressions are constructed using the *a priori* spectral estimate at each iteration m. This approach approximates the underlying spectrum using the current best estimate, which is then substituted into the variance expression for the single-segment estimator. Expressions for the expectation and variance of the rth-root transformed multitaper estimator are provided in Eqs. (7) and (8), which follow directly from the nth moment of $\hat{S}$ as provided in Thomson (2000). $\Gamma(\bullet)$ denotes the Gamma function. The periodogram approach may be considered by substituting the number of degrees-of-freedom $\nu = 2$ into the relevant expressions.

$$\mathrm{E}\{\hat{S}^{1/r}\} = \left(\frac{2S}{\nu}\right)^{1/r} \frac{\Gamma(\nu/2 + 1/r)}{\Gamma(\nu/2)} \tag{7}$$

$$\mathrm{var}\{\hat{S}^{1/r}\} = \left(\frac{2S}{\nu}\right)^{2/r} \left(\frac{\Gamma\left(\nu/2 + 2/r\right)}{\Gamma(\nu/2)} - \frac{\Gamma^2(\nu/2 + 1/r)}{\Gamma^2(\nu/2)} \right). \tag{8}$$

Table 1
Optimal root-transform for multitaper estimators of νdegrees-of-freedom

ν	1	2	4	6	8	10	12	14	16
r	4.34	3.60	3.27	3.17	3.12	3.10	3.08	3.07	3.06

Results shown to two decimal places for a selection of ν values.

Note that while the untransformed spectra are asymptotically unbiased, both logarithmic and rth-root transforms produce biased results. Substituting the unbiased estimate of $S^{1/r}$ into Eq. (8) reveals a direct estimate of the variance as

$$\widehat{\mathrm{var}}\{\hat{S}^{1/r}\} = \hat{S}^{2/r}\left(\frac{\Gamma(\nu/2)\Gamma(\nu/2+2/r)}{\Gamma^2(\nu/2+1/r)} - 1\right). \quad (9)$$

In order to determine an appropriate choice for r we require a measure of symmetry. Skew is a measure of the asymmetry of a distribution and is thus ideally suited to the task at hand. Appendix A provides a derivation for the skew of a rth-root transform multitaper estimator and shows that the result is independent of S. Thus, given a choice of ν it should be possible to determine the value of r that produces the optimal skew-symmetric distribution. A perfectly symmetrical distribution will produce a skew of zero given, for root-transformed spectra, as

$$\Gamma^2\left(\frac{\nu}{2}\right)\Gamma\left(\frac{\nu}{2}+\frac{3}{r}\right) - 3\Gamma\left(\frac{\nu}{2}\right)\Gamma\left(\frac{\nu}{2}+\frac{1}{r}\right)\Gamma\left(\frac{\nu}{2}+\frac{2}{r}\right) + 2\Gamma^3\left(\frac{\nu}{2}+\frac{1}{r}\right) = 0. \quad (10)$$

This equation may be solved numerically to a sufficient approximation, i.e. two decimal places. The optimal skew-symmetry choice for r is provided for a selection of degrees-of-freedom ν in Table 1.

Table 1 shows a clear convergence towards the cube-root with increasing ν, justifying the cube-root as a suitable symmetric distribution for multitaper estimates (as suggested in Thomson and Chave, 1991). For periodogram estimates however, the choice of $r = 3.60$ for $f \neq \{0, (1/(2\Delta t))\}$ is a sufficient distance from the cube-root to justify its use. In addition, the tracking of periodogram ordinates at $f = \{0, (1/(2\Delta t))\}$ would require a root-transform of $r = 4.34$ to achieve symmetry.

2.7. Confidence limits

The framework for optimal spectral tracking lends itself to a variety of implementation strategies in the derivation of confidence intervals. At the fore of these methods is the empirical approach, in which the mean and variance of the filter output (provided by the *a posteriori* state and error-covariance matrix) are utilised directly in the placement of confidence intervals. As the output of a Kalman filter is normally distributed the mean and variance are sufficient statistics for the determination of a confidence interval. Limits may then be transformed to the frequency domain as required.

Confidence limits derived from the output of a Kalman filter will rely on the accuracy of the distributional assumptions imposed on the input data. Specifically, it is required that the transformed single-segment estimator is approximately normal. The distribution of the periodogram for $f \neq 0, 1/(2\Delta t)$ is proportional to χ^2_2. Fig. 2 demonstrates that $\ln(\chi^2_2)$ provides a statistic approaching the normal assumption, while multitaper methods improve this distributional approximation. Any non-normality in the initial state will rapidly dissipate in the filtered output due to convergence under the central limit theorem.

Numerical methods are now discussed in a comparative study, with a focus on jackknife and Monte-Carlo approaches. Jackknife procedures are reviewed in application to periodogram and multitaper estimates in Thomson and Chave (1991). Jackknifing may be performed over trials by a renormalisation of filter weights (necessary for smoothing) for each delete-one estimate. Appropriate variance stabilising transforms are applied during the jackknife procedure. For spectra the log-transform is appropriate, while Fisher's z-transform of magnitude coherency $\tanh^{-1}|R_{xy}(f)|$ leads to a measure which may subsequently be transformed to coherence.

Monte-Carlo simulations may be considered where the spectral tracking framework affords a convenient implementation strategy through single process evaluation. To maximise the number of independent frequency components computed per process realisation, surrogate data are generated for a single-channel Gaussian white noise process. Under these conditions, spectral components will remain uncorrelated (with sufficient down-sampling should multitaper estimates be employed). Since spectral statistics are independent of trial length, relatively long segments may be chosen to provide a set of frequencies appropriate for Monte-Carlo averaging. For example, utilising periodogram estimates for a series of segments, each of length 2×10^4 samples, will produce 10^4 uncor-

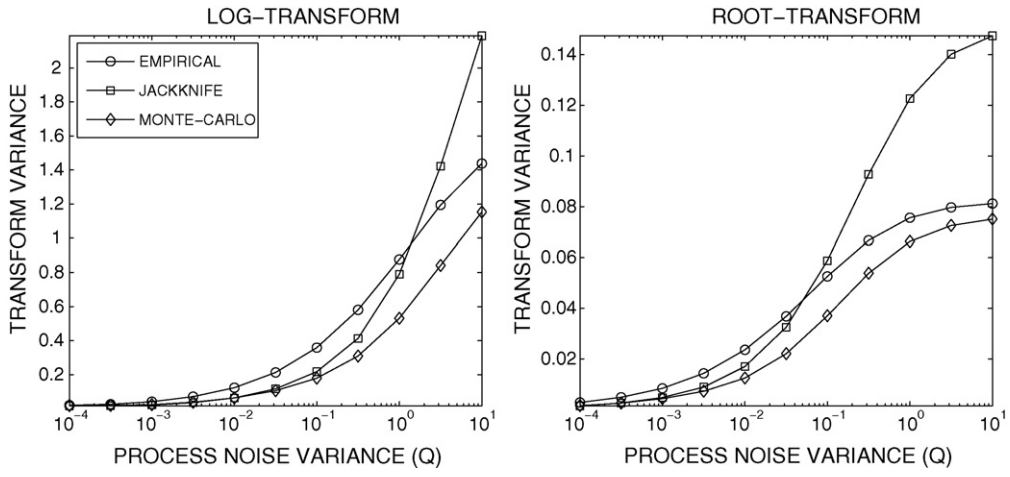

Fig. 4. Variance of transformed spectra derived from empirical and numeric approaches. Variance determined from the power spectrum of a single-channel i.i.d. standard normal process ($\mathcal{N}(0, 1)$). Results displayed for empirical, jackknife and Monte-Carlo methods, applied to logarithmic (left) and root-transform (right) data.

related spectral components per trial. Statistical inference may then be considered across frequencies at each trial recursion, thus leading to numerical evaluation within a single implementation of the tracking framework.

The behaviour of confidence limits derived from empirical and numerical methods are now considered. Fig. 4 displays the variance of power-spectrum estimates corresponding to a single channel i.i.d. standard normal process ($\mathcal{N}(0, 1)$). Variance is derived using empirical (see above description), jackknife and Monte-Carlo methods for both the natural logarithm and rth-root transform. For implementation within the spectral tracking framework, data were segmented into 100 trials each of length 1000 samples and processed using periodogram methods. Variance was determined on the output of the final (100th) trial, averaged across frequencies. Output variance is computed for changing input noise variance Q (a scalar in this case) over the logarithmic scale $Q = 10^n$ for $n = -4, \ldots, 1$.

The variance of the log-periodogram ordinate for $0 < f < 1/(2\Delta t)$ is given by $\psi'(1) = 1.6449$ to [4 d.p.]. The variance of the root-transform periodogram ($\nu = 2$) for $r = 3.60$ corresponding to a standard normal process within $0 < f < 1/(2\Delta t)$ is 0.0773 [4 d.p.] (applying Eq. (8)). From Fig. 4 it is evident that variance estimates improve as Q becomes small, i.e. tracking reduces to the sample mean. For estimates below 10^{-1} all three variance estimates are in close correspondence. We place greatest trust in Monte-Carlo simulations since they are free of distributional assumptions and are computed directly from the data over a large ensemble, though limited here to Gaussian white noise processes. Ultimately however, Monte-Carlo simulations can only reliably correspond to data possessing an equivalent distribution. With this in mind it is clear that empirical limits consistently over-estimate the variance of the output process. We do not consider the overestimate to be severe however as this would lead to liberal confidence intervals, thus representing an efficient first approximation for significance testing.

Jackknife limits appear much closer to their numerical Monte-Carlo counterparts for low level process noise. When process noise variance approaches that of the single-segment estimator (1.64 for log-periodogram, 0.08 for root-periodogram), local smoothing is severely reduced leading to a small number of estimates. Jackknife procedures require a large number of single-segment estimators to effectively estimate variance, thus the jackknife approach is undermined. For process noise variance smaller than that of the single-segment estimator, jackknife limits appear to approximate the underlying statistics well (determined through Monte-Carlo methods). In what follows the log-periodogram approach is adopted with process noise variance Q varying between 0.001 and 0.1, a range which provides accurate variance estimation by jackknife methods.

3. Results

3.1. Application to surrogate data

To demonstrate the tracking and smoothing capabilities of optimal Kalman filtering, time-series are constructed with a known coherence relationship. These data are then analysed using both tracking and smoothing techniques.

The two signals $s_1(t)$ and $s_2(t)$ are constructed in similar fashion to Lachaux et al. (2002)

$$s_1(t) = \epsilon_1(t) + \alpha(t)\epsilon_2(t)$$
$$s_2(t) = \alpha(t)\epsilon_1(t) + \epsilon_2(t)$$
$$\alpha(t) = \frac{1}{2}[1 + \cos(2\pi f_a t)]$$

with $\epsilon_1(t)$ and $\epsilon_2(t)$ i.i.d. Gaussian white noise processes with zero mean and unit variance $\mathcal{N}(\mu = 0, \sigma^2 = 1)$. The cross-correlation function between signals $s_1(t)$ and $s_2(t)$ can be derived as a function of $\alpha(t)$ as

$$\rho(t) = \frac{2\alpha(t)}{1 + \alpha(t)^2}. \quad (11)$$

We now attempt to track the changing correlation structure between signals $s_1(t)$ and $s_2(t)$ in the frequency domain through use of a time-varying coherence function, computed in trial-wise fashion. A total of 100 s of data were simulated at a sampling rate of 1 kHz using $f_a = 0.06$ Hz. To facilitate analysis within the optimal spectral tracking framework the data is segmented into disjoint sections of length 200 ms. Fig. 5 shows the analytic coherence (Eq. (11)) along with estimates obtained via Kalman tracking and smoothing of the spectra for a single realisation of the process utilising the log transform periodogram. Estimated coherence values represent activity centred about the 10 Hz component, given a Rayleigh resolution of 5 Hz (note that the process is frequency-shift invariant).

Kalman filtering methods provide a good approximation to the data, with some small inevitable tracking lag. Kalman smoothing addresses the issue of tracking lag, but are subsequently less capable of characterising transient changes. Visual examination of the figures suggest oscillatory coherence with a period of approximately 80 segments. Given the duration of each segment we determine a coherence rhythm of 0.0625 Hz, in close agreement with the known analytic model. Note that process noise variance was not selected to precisely fit the analytic model, but instead represents typical tracking performance to be expected through manual parameter tuning.

3.2. Variable speed treadmill locomotion

A number of studies have attempted to explore the neural-dynamics of locomotion (e.g. Murray et al., 1984; Nielsen and Kagamihara, 1994; Grasso et al., 1998; Hansen et al., 2001, 2005; Nielsen et al., 2005; Gazendam and Hof, 2007). One of the simplest and most accessible control variables during treadmill locomotion is that of locomotor speed. In many experiments subjects are permitted to walk at a comfortable pace (i.e. Grasso et al., 1998; Hansen et al., 2001, 2005; Gazendam and Hof, 2007). Others fix this parameter as a potential source of inconsistency. The adjustment of locomotor speed from a subjects natural walking pace is known to produce significant differences in gait kinematics (Murray et al., 1984), implying a change in neural drive.

A key question in human physiology is the existence of modulatory neural control systems that influence or are influenced by locomotor speed. Determining and characterising such mechanisms would provide key insights into the organisation of the nervous system and motor control. Such modulatory rhythms would also provide a possible explanation for the wide-ranging inter-subject variability observed during studies conducted at comfortable walking pace (differences in locomotor speed) and fixed walking pace (artificial control).

3.3. Data

Five subjects were recruited to participate in treadmill walking. Belt speed was modulated in an orderly manner. All subjects were familiarised with treadmill walking prior to testing. Recordings consisted of a 540 s period split into three equal parts, an accel-

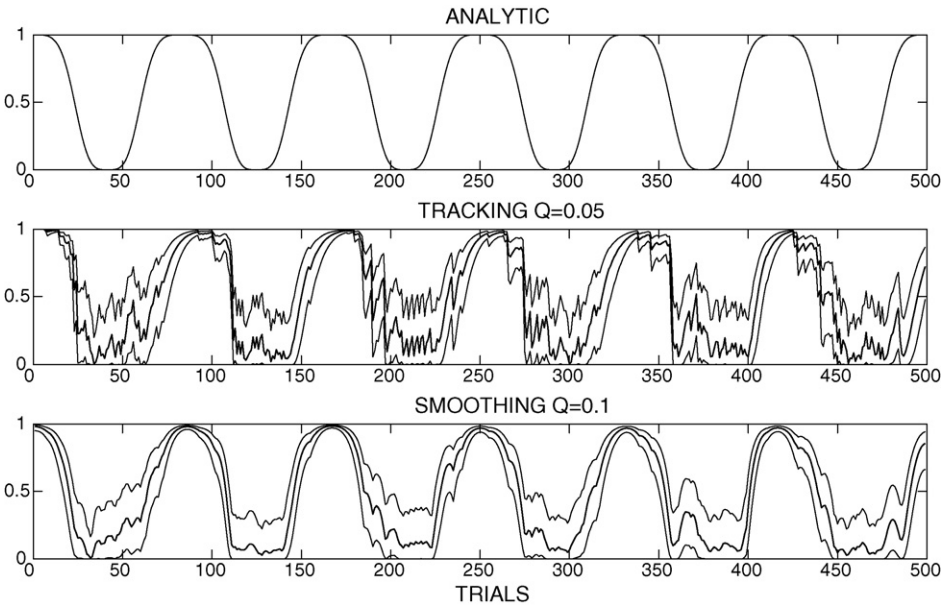

Fig. 5. Evolutionary coherence shown for the analytic value with coherence oscillating at 0.06 Hz, the Kalman tracking estimate with $Q = 0.05$ and the Kalman smoothing estimate with $Q = 0.1$. Estimated coherence values displayed with 95% confidence intervals determined through jackknife procedures.

eration period, a constant velocity period and finally a deceleration period.

Paired bipolar surface electromyogram (sEMG) recordings (Ag–AgCl blue sensor electrodes) were taken from two sites on the tibialis anterior muscle (ankle flexor) corresponding to upper (proximal) and lower (distal) portions of the muscle. These regions of TA are believed to be innervated by independent populations of motor axons arising from the tibialis anterior motoneurone pool (Hansen et al., 2001). Force Sensitive Resistors (FSR) were attached to the heels of both feet to identify heel strike during locomotion. All data were sampled at 1 kHz.

Triggers were extracted from the force record based on heel offloading, which occurs just subsequent to the onset of TA activity, with heel strike approximating the TA inactivation time. These epochs do not directly specify the TA activation region, but will prove useful in its determination. It was found that during very slow treadmill speeds, subjects demonstrated highly heterogeneous locomotor gait patterns. These were found to normalise at approximately 2.2 km/h once a more natural walking pace had been attained. We therefore rejected all epochs corresponding to treadmill speeds of less than 2.2 km/h.

3.4. Results

Tibialis anterior is an ankle flexor, active predominantly during the swing phase of the step-cycle. The swing phase is known to shorten during periods of increased walking pace (Kandel et al., 2000). This leads to inconsistent epoch lengths. The underlying assumption required to compare trials of inconsistent length is that the structure of each trial is proportioned relative to the length of that trial. This implies that the underlying neural mechanisms operating over periods of muscle contraction occur in proportion to the duration of burst activity. By representing burst activity on a normalised time-base (through the application of NAEs), epochs should bear similarity in their time-course of activation. To evaluate this assumption in relation to TA activation, separate NAEs were constructed for the constant and variable speed trials. The constant speed trials are those that occur between 180 and 360 s at a speed of 4 km/h. Variable duration trials include those from the linear increase and decrease sections, specifically between 0–180 and 360–540 s. A combined NAE consisting of all trials is then constructed. Sample NAEs are displayed for lower left TA from the first run of Subject 1 in Fig. 6.

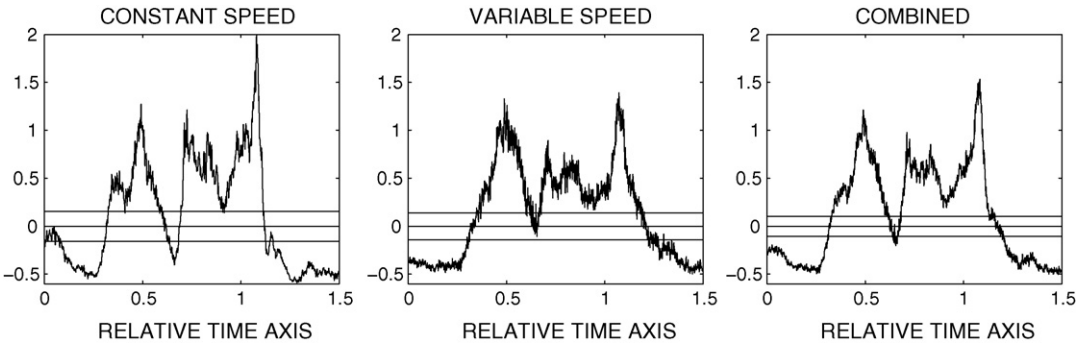

Fig. 6. Normalised activity envelopes for lower left TA from the first run of Subject 1. NAEs correspond (left-to-right) to constant speed trials, variable speed trials and a combination of both constant and variable speed trials. Horizontal lines depict the origin and 95% confidence interval under the null hypothesis of independence.

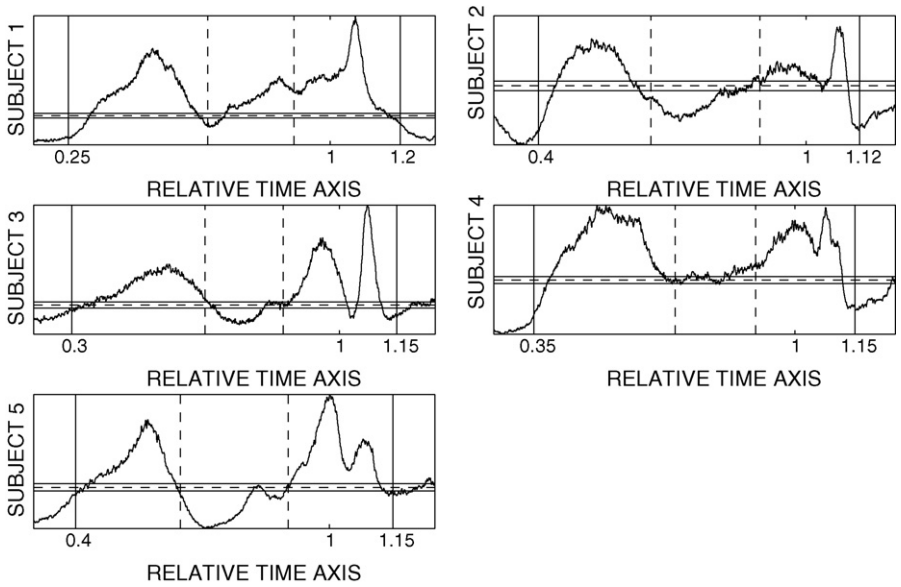

Fig. 7. Average activity envelopes showing relative increase in TA activity. Sample envelopes are shown for Subjects 1–5 ramp1 lower left TA. Time points $0 \rightarrow 1$ indicate normalised heel contact with the treadmill belt, while the solid vertical lines indicate the chosen TA activity envelope for subsequent analysis. Dashed horizontal lines denote the zero line with solid horizontal lines the 95% confidence interval under the null hypothesis of independence.

A total of 160 trials were included in the constant speed NAE of Fig. 6, with 192 in the variable speed section. Combined results included all trials of constant and variable speed, resulting in a count of 352. The constant speed NAE of Fig. 6 displays a well defined activity envelope with prominent time-localised features. Envelope shape may be considered in analogy with healthy treadmill locomotion (i.e. Kandel et al., 2000; Halliday et al., 2003), consisting of three clear bursts of activity. The first burst occurs between relative time points 0.25 and 0.65, the second between 0.65 and 0.9 and the third between 0.9 and 1.15. Addi-

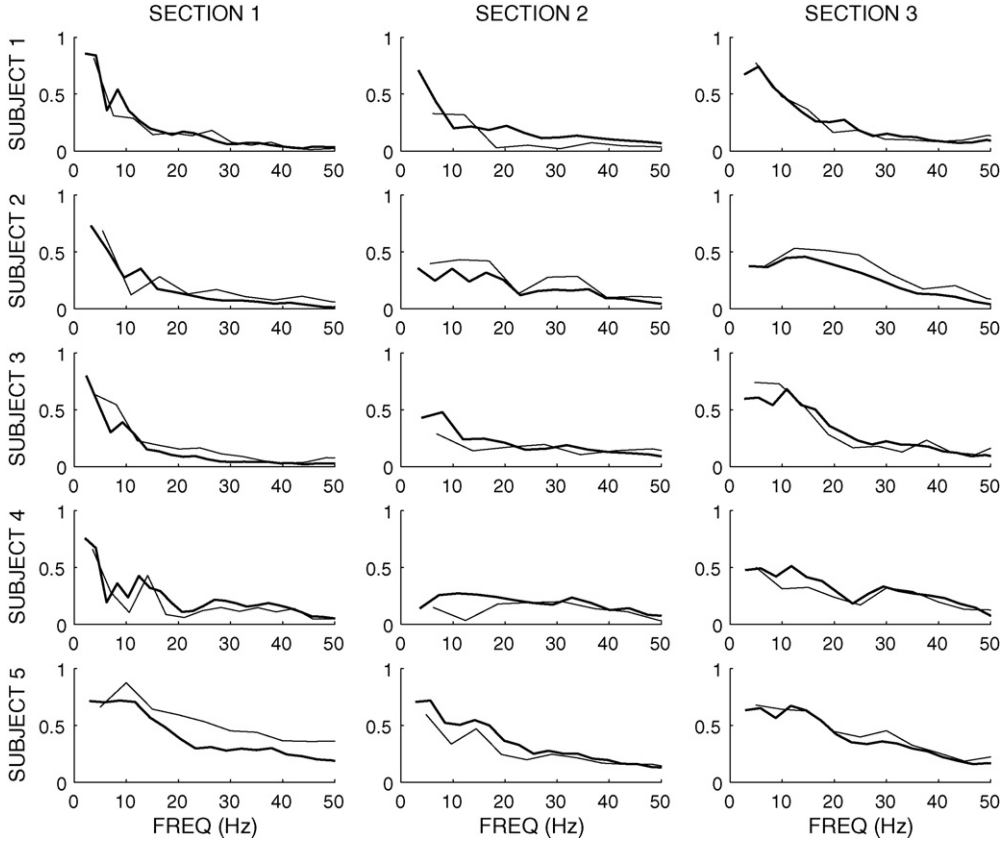

Fig. 8. Coherence determined through traditional trial-average spectra. Columns correspond to sections (1–3), while rows represent subjects. Thin lines denote coherence derived from constant speed locomotion (4 km/h). Bold lines represent coherence derived across all trials.

tional short-term structure is also evident riding on these primary features.

Trials over variable speeds produce an NAE with similar form to those corresponding to constant speed (see Fig. 6). The three primary bursts are evident, though features appear slightly less well defined. The slight loss of localisation is most evident during the inactive period around relative time offset 0.65 and the strong peak in the vicinity of heel strike at relative offset 1.1. These characteristics are to be expected since longer trials will naturally result in a moderate relaxation of feature alignment. The combined constant and variable speed NAE characterises the relative common activity envelope produced during the experiment. As may be expected, it resembles a weighted combination of the constant and variable speed NAEs. The similar structure of NAEs corresponding to variable speed, constant speed and combined trials provides a clear indication that the time-course of motor activity may be considered well defined on a normalised time-base.

In determining increased regions of TA activation, NAEs were constructed for all experiments. It was found that activity envelopes calculated for experiments from the same subject showed marked similarities. Likewise, TA envelopes from either limb of the same experiment show near identical modulation. Fig. 7 shows the NAEs for each subject, combining epochs from the left and right sides. Average envelopes are displayed on a normalised time scale, where 0 corresponds to the trigger (heel raised from treadmill belt), and 1 corresponds to the end of the epoch (heel strike). The solid vertical lines in Fig. 7 delineate the region of increased TA activity, marked by visual examination.

In characterising non-stationary behaviour within the dataset we must consider modulation within trials as well as across trials. We term these conditions relative- and real-time non-stationarity. Real-time non-stationarity results from the experimental protocol, where locomotor speed is varied across trials. Relative-time non-stationarity arises from dynamic changes in pre-synaptic drive to motorneurones during the relative phases of the step-cycle.

To aid the characterisation of relative-time non-stationarity, TA activity is divided into three segments. These three segments are chosen by visual examination of the activity envelopes (see Fig. 7). Segmentation is chosen to match the physiological modulation of TA activity during the step-cycle, with a focus on early and late bursts corresponding to periods of increased motor-neuronal drive. Each experiment is segmented individually to allow for inter-subject variability in burst duration.

Before examining any speed-modulated features, traditional trial-average spectra (Bloomfield, 2000) were computed for the three segment analysis. Results of a coherence analysis are displayed in Fig. 8, where spectra were computed across all trials as well as for the specialised case of constant speed locomotion (those recorded at 4 km/h).

Results from Fig. 8 demonstrate similarity in general coherence trends between constant speed locomotion and the more general case of variable speed locomotion. Section 1 highlights a peak within the 7–9 Hz band evident across all five subjects. Sections 2 and 3 display broadband coherence with peaks in individual coherence spectra, inconsistent between subjects. These results are in agreement with previous findings, e.g. Halliday et al. (2003).

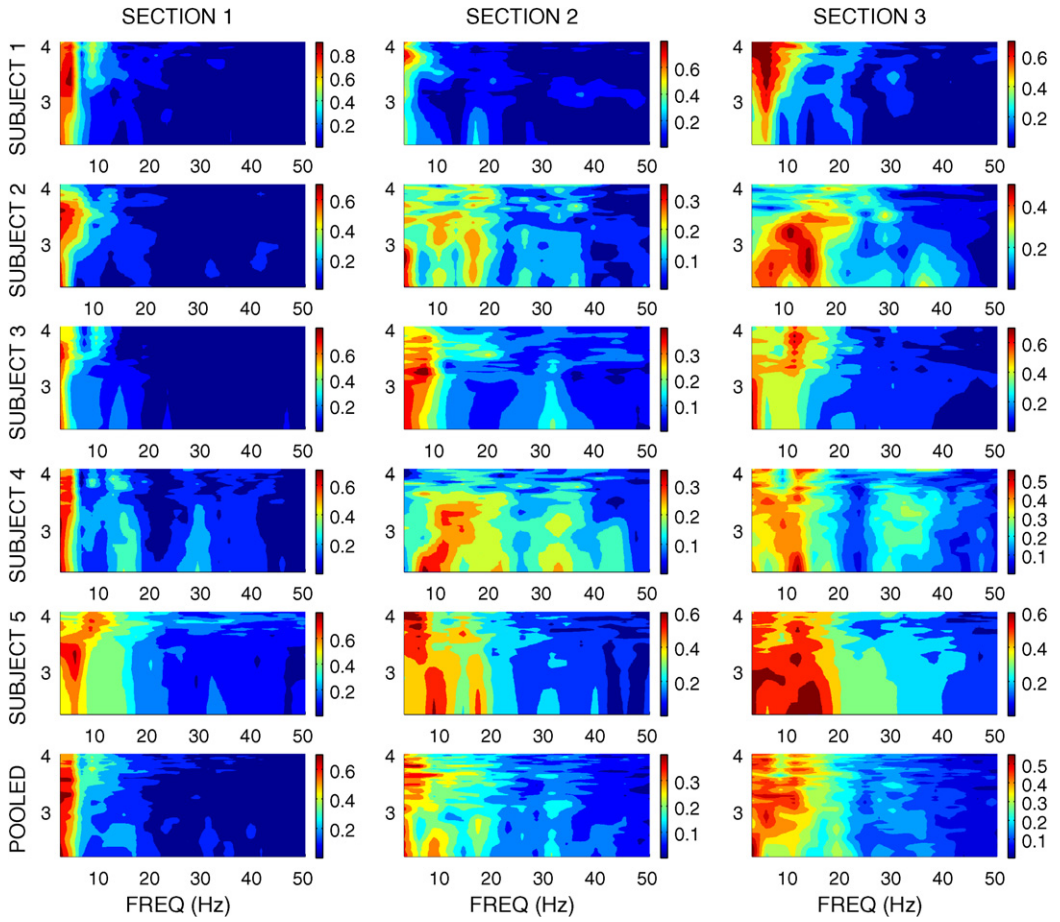

Fig. 9. Coherence produced by optimal spectral smoothing over individual subjects (rows 1–5) and pooled over all subjects (row 6). Individual subjects were analysed using $Q = q\mathbf{I}$ with $q = 0.002$, with $q = 0.0005$ for the pooled measure. Columns represent the three segments of the active region. Ordinates correspond to treadmill speed.

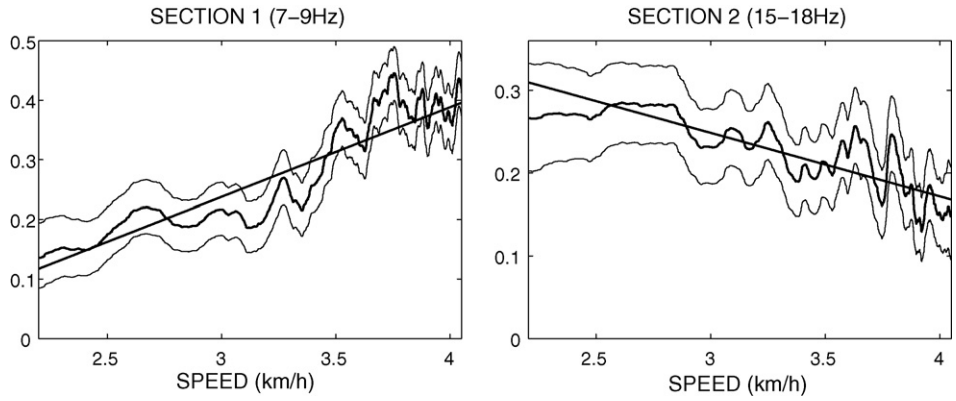

Fig. 10. Coherence obtained within specified frequency bands. Left figure denotes 7–9 Hz activity for pooled section 1. Right figure denotes 15–18 Hz activity for pooled Section 2. Coherence displayed with pointwise jackknife confidence intervals at the 95% interval. Regression line fit to obtain the minimum-mean-square error.

Variation in results may reflect a high degree of inter-subject variability, but may also be due to a modulating locomotor drive. Examination with optimal spectral tracking may help clarify this discrepancy.

Optimal spectral tracking was performed using the computationally efficient log-transform periodogram as single-segment estimator. The periodogram approach maintains frequency resolution over its multitaper counterpart. Analysis using the appropriate root-transform method was also considered, producing near identical results in all cases.

Spectra and coherence were produced through optimal spectral smoothing ($Q = q\mathbf{I}$ with $q = 0.002$) between upper and lower TA EMGs, pooled across left and right sides for each subject. Coherence results, corresponding to a three-segment analysis, are displayed in Fig. 9. In ordering and plotting trials by locomotor speed we hypothesise that coherence activity within certain frequency bands modulate in a speed dependent manner.

In assessing any unpredicted spectral bias that might result from the proposed method, all data were replaced by i.i.d. Gaussian white noise, while retaining trigger times and epoch lengths. In essence, the structure of each trial was retained while replacing the EMG signal with surrogate data. Optimal spectral tracking and smoothing procedures were repeated on the surrogate dataset, where spectra and coherence showed no discernible bias in magnitude towards either high or low speed trials. This provides further evidence that the features extracted using spectral tracking represent dynamic changes in the structure of the signal, as opposed to bias from the method.

Returning to the physiological data, Fig. 9 demonstrates clear regions of speed-modulated coherence. Several features appear consistent across subjects, while others appear significant in only a few subjects. This may well reflect the high degree of inter-subject variability typically evidenced in locomotor gait (Halliday et al., 2003; Gazendam and Hof, 2007). In identifying common changes, subjects were pooled to include all data from both sides and optimal spectral smoothing applied with $q = 0.0005$. Pooled results are presented on the bottom row of Fig. 9 for a three-segment analysis.

The pooled results of Fig. 9 provide an overview of the data which may be utilised in conjunction with individual subject estimates to identify common modulatory changes. Both pooled and individual results demonstrate a strong unmodulated component dominating the sub-5 Hz frequency range in section 1. Following subsequent tests (which include thresholding the rectified data) this feature has been attributed to envelope modulation. High levels of coherence also support this conclusion.

Various other features appear to modulate both with and against treadmill speed. The 7–12 Hz band previously identified from Fig. 8 appears to increase with locomotor speed. By plotting the midpoint of this range, a trace of coherence activity may be extracted in relation to locomotor pace while facilitating the placement of confidence intervals, as previously described. Activity in the 7–9 Hz range is provided in Fig. 10, obtained by selecting the 8 Hz component given a bandwidth of 2 Hz. We see that 7–9 Hz coherence demonstrates strong positive correlation with locomotor speed (linear regression coefficient $\alpha_1 = 0.15$, correlation coefficient $r = 0.79$). Despite strong correlations, we restrict our interpretation of regression analysis as indicative only, aiding the identification of general trends in the data. Indeed, close examination of Fig. 10 in conjunction with Fig. 9 suggest several non-trivial relationships.

The other frequency band displaying significant modulation in the majority of subjects (4 out of 5) is 15–18 Hz during section 2. The right panel of Fig. 10 displays a frequency slice taken from the pooled dataset through 16.5 Hz given a bandwidth of 3 Hz. Examination of Fig. 10 indicates a gradual near linear change, negatively correlated with locomotor speed ($\alpha_1 = -0.07$, $r = 0.80$). This demonstrates the presence of speed-modulated coherence in both a positive and negative direction.

In addition to these components, various modulating rhythms are evident in individuals or across a selection of subjects. In section 2 for instance, 7–12 Hz activity appears to correlate negatively with speed in 2/5 subjects. This is in direct opposition to the positive correlation observed across the majority of subjects in section 1. There is also a 30–35 Hz component, also negatively correlated with speed in 3/5 subjects, with one further subject demonstrating a similar pattern but with an associated increase in coherence at faster treadmill speeds.

It is sometimes also useful to plot coherence modulation across concatenated experiments where smoothing has been applied to the unsorted trials. In the present analysis we consider coherence against trial number, and overlay a speed vector for feature extraction. Concatenating unsorted trials is justified given the experimental protocol, where the final speed of locomotion returns to its initial level. Such figures also provide an indicator to anomalous experiments or subjects with peculiar locomotor patterns.

To highlight the substantial effects of inter-subject variability, a frequency slice diagram was constructed for section 1 of the variable speed locomotion dataset, displayed about $f = 5$ Hz (bandwidth 2 Hz) in Fig. 11. Speed vectors were smoothed for each trial using the associated Kalman derived weight matrix. This provides a more direct indication as to the average speed considered per trial while reducing fluctuations about mean activity thus leading to a

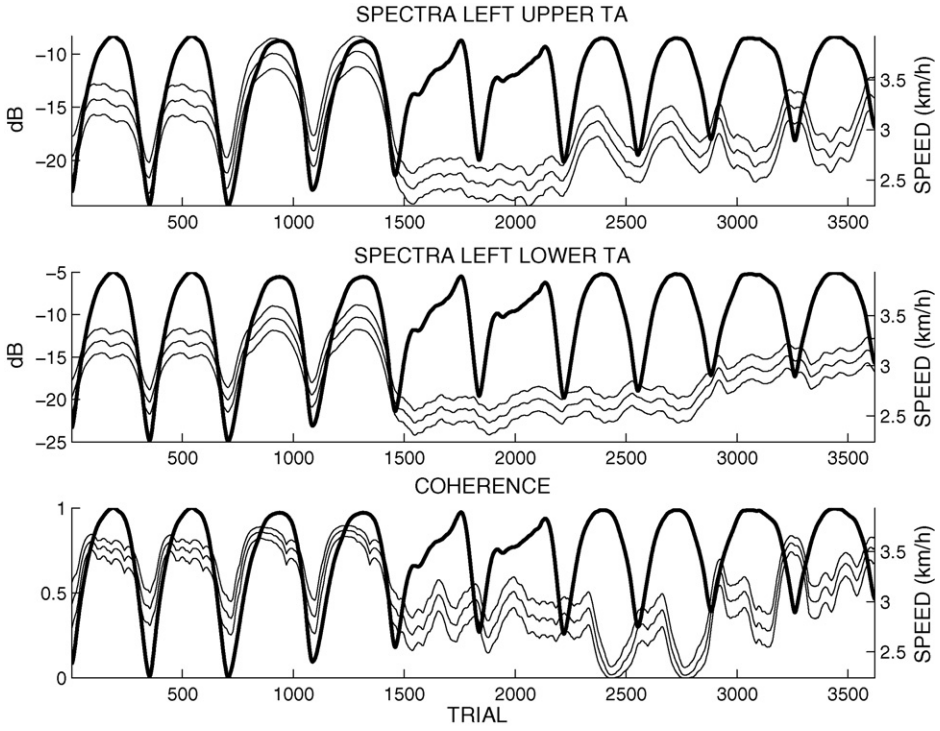

Fig. 11. Frequency slice at $f = 5$ Hz for pooled unsorted spectral smoothing. Smoothing process noise $q = 0.002$. Thin solid lines denote spectra and coherence. Dashed lines denote the 95% jackknife confidence interval. Thick lines denote average locomotor speed and correspond to the right-side axis. Figure corresponds to start section 1 of 3. Subjects 1 and 2 show coherence strongly modulated with locomotor speed. Subject 3 does not show significant signs of coherence modulation and Subjects 4 and 5 show negatively correlated modulation.

clearer representation. Note that coherence levels are extremely similar between pairs of experiments from the same subject, with inter-subject variability producing substantial fluctuations. There is also some unusual activity in the speed vector of subject 3. This should not unduly affect analysis of sorted trials as the calculated speed vector will ensure appropriate ordering.

Fig. 11 displays variability in spectra and coherence modulation with locomotor speed. For Subjects 1 and 2 the modulation is strongly correlated with locomotor speed for both spectra and coherence. For Subject 3 the modulation is not so evident, and for Subjects 4 and 5 modulation appears to indicate a strong negative correlation, i.e. modulation with the inverse of locomotor speed. These results demonstrate that coherence activity is modulated by locomotor speed within certain frequency bands. It is also evident that there exists a high degree of inter-subject variability in speed-modulated locomotor gait.

4. Discussion

A novel method of optimal spectral-tracking and smoothing has been presented for the characterisation of trial-varying parameters. Confidence limits have been derived and considered alongside those determined through numerical methods. The framework has been applied to surrogate data where results were in agreement with the underlying model (Fig. 5). These methods were subsequently utilised in characterising the changing neural locomotor drive of tibialis anterior during variable speed treadmill walking in humans.

The inapplicability of traditional STA measures for trials of inconsistent length motivated the constructed of a mean measure of activity projected onto a normalised time-base. This measure was dubbed a Normalised Activity Envelope, providing the time-course of activation for TA muscle contraction over the variable speed locomotor experiment.

Though preliminary, the present study has demonstrated clear modulation of TA in relation to treadmill speed. The early period of TA contraction (section 1), corresponding to early swing, includes a 7–12 Hz component, positively correlated with speed (Fig. 10). This is concentrated around 7–9 Hz, with one subject showing a shift in frequency closer to 9–12 Hz. Similar structure was identified both in the trial-average analysis of the present dataset (Fig. 8) and in previous investigations (Halliday et al., 2003).

In section 2, the 15–18 Hz component identified as negatively correlated with locomotor speed appears innocuous in the trial-average analysis. This highlights a rhythm demonstrating a changing dynamic that is not fully represented in traditional trial-average analysis. Likewise, numerous modulating rhythms appear, isolated within 1 or 2 subjects. The potential for spectral tracking to elicit speed modulating rhythms encourages progress in this area, including foremost, a more exhaustive set of experiments focused about our present findings. While a focus has been drawn in the current report to modulating rhythms, spectral tracking has clarified the role of numerous other frequency constituents which remain speed invariant.

Prior investigations into TA modulation with locomotor speed in man (Hansen et al., 2001) have involved the placement of multiunit wire electrodes in conjunction with surface EMG. Results concluded that no significant change in either short-term synchronisation or general synchrony could be observed between pairs of TA electrodes from the homonymous muscle. Additionally, a clear 15–18 Hz peak in coherence was observed over the duration of muscle contraction. Present findings suggest that while general synchrony remains relatively unaffected, the effect within spe-

cific frequency bands may be marked. Indeed, modulating rhythms likely reflect a change in dynamic of the CPG system, coordinated though descending control. The findings of Hansen et al. (2001) also suggest that any short-term synchrony measures may well remain unchanged.

Optimal spectral smoothing has identified speed-modulated coherence rhythms (see Figs. 9 and 10), present within TA-EMG during the active phase of the step-cycle. These were previously unidentified due to limitations in the analysis methodology and a focus on constant speed locomotion. Prior investigations have noted a high degree of variability between subjects, especially in the initial stage of TA activation (Alton et al., 1998; Halliday et al., 2003).

Consideration of alternate treadmill locomotion protocols would allow for a wide range of hypotheses to be tested. For instance, by progressively inclining the treadmill belt (achievable through pneumatic ramps), work load may be assessed while maintaining a constant locomotor pace. The tracking of motorneural drive under ramp inclination may reveal CPG responses to an increase in work load.

The generality of the proposed optimal spectral tracking framework make these methods applicable to a wide range of characterisation studies. As well as repeat trial experiments, where a control parameter is adjusted over epochs, spectral tracking provides the capability of detecting non-stationarity within extended single-trial data (as demonstrated by the surrogate data example of Section 3.1). The optimal spectral tracking framework quantifies trial-variability and encourages the development of more complex experimental protocols. The prospect of moving away from the traditional repeat-trial philosophy opens new avenues to investigate the control mechanisms influencing many neurophysiological signals such as EEG or MEG. Though stated in the framework of periodogram and multitaper estimates, a natural progression appears to exist to both wavelet (Percival and Walden, 2000) and multi-wavelet (Brittain et al., 2007) methods.

Acknowledgements

We wish to thank the two referees for their helpful and insightful comments. This work was supported by the BBSRC, grant number 10477.

Appendix A. Invariance of skew to the underlying spectrum

A multitaper estimate $\hat{S}$ possesses a distribution of $(S/\nu)\chi^2_\nu$. This leads to the μth-raw moment of the rth-root transform estimator as defined in Eq. (12), hereafter denoted γ'_μ, dropping the dependence on r for notational convenience

$$\gamma'_\mu = \mathrm{E}\{\hat{S}^{\mu/r}\} = \left(\frac{2S}{\nu}\right)^{\mu/r} \frac{\Gamma((\nu/2)+(\mu/r))}{\Gamma(\nu/2)}. \tag{12}$$

Skew is a measure of the degree of asymmetry of a distribution, defined in terms of central moments γ_μ as

$$\frac{\gamma_3}{\gamma_2^{3/2}} \tag{13}$$

which may be expressed in raw moments as

$$\frac{\gamma'_3 - 3\gamma'_1\gamma'_2 + 2\gamma'^3_1}{(\gamma'_2 - \gamma'^2_1)^{3/2}}. \tag{14}$$

Substituting Eq. (12) for the raw moments we determine the skew for the rth-root transform multitaper (and periodogram) estimator as

$$\frac{(2S/\nu)^{3/r}((\Gamma((\nu/2)+(3/r)))/(\Gamma(\nu/2))) - 3(2S/\nu)^{3/r}((\Gamma((\nu/2)+(1/r))\Gamma((\nu/2)+(2/r)))/(\Gamma^2((\nu/2)))) + 2(2S/\nu)^{3/r}((\Gamma^3((\nu/2)+(1/r)))/(\Gamma^3(\nu/2)))}{((2S/\nu)^{2/r}((\Gamma((\nu/2)+(2/r)))/(\Gamma(\nu/2))) - (2S/\nu)^{2/r}((\Gamma^2((\nu/2)+(1/r)))/(\Gamma^2(\nu/2))))^{3/2}}. \tag{15}$$

After tidying the $(2S/\nu)$ terms cancel leaving

$$\frac{\Gamma^3(\nu/2)[\Gamma^2(\nu/2)\Gamma((\nu/2)+(3/r)) - 3\Gamma(\nu/2)\Gamma((\nu/2)+(1/r))\Gamma((\nu/2)+(2/r)) + 2\Gamma^3((\nu/2)+(1/r))]}{\Gamma^3(\nu/2)\Gamma^3((\nu/2)+(2/r)) - 3\Gamma^2(\nu/2)\Gamma^2((\nu/2)+(2/r))\Gamma^2((\nu/2)+(1/r)) + 3\Gamma(\nu/2)\Gamma((\nu/2)+(2/r))\Gamma^4((\nu/2)+(1/r)) - \Gamma^6((\nu/2)+(1/r))}. \tag{16}$$

The resulting expression is dependent entirely on (ν, r). Since ν is chosen prior to analysis, skewness for a particular choice of ν will remain constant regardless of the underlying spectral density function. The optimal choice of skew-symmetry thus occurs when the above expression is equal to zero, i.e. when the numerator is zero (assuming a non-zero denominator). The numerator may be factorised into two parts, one of which being $\Gamma^3((\nu/2))$. Since ν is chosen positive and $\Gamma(x) > 0$ for $x > 0$, the optimal choice of r must be determined through the remaining factor of the numerator, namely Eq. (10). The solution may be determined numerically to a sufficient approximation, i.e. two decimal places in this case.

References

Alton F, Baldey L, Caplan S, Morrissey MC. A kinematic comparison of overground and treadmill walking. Clin Biomech 1998;13(6):434–40.
Bloomfield P. Fourier analysis of time series: an introduction. New York: Wiley; 2000.
Brillinger DR. Time series: data analysis and theory—expanded edition. CA: Holden Day; 1981.
Brittain J-S, Halliday DM, Conway BA, Nielsen JB. Single-trial multi-wavelet coherence in application to neurophysiological time series. IEEE Trans Biomed Eng 2007;54:854–62.
Brown RG, Hwang YC. Introduction to random signals and applied Kalman filtering. New York: Wiley; 1997.
Drake AW. Fundamentals of applied probability theory. Ohio: McGraw-Hill; 1967.
Gazendam MGJ, Hof AL. Averaged EMG profiles in jogging and running at different speeds. Gait Posture 2007;25(4):604–14.
Grasso R, Bianchi L, Lacquaniti F. Motor patterns for human gait: backward versus forward locomotion. J Neurophysiol 1998;80(4):1868–85.
Halliday DM, Rosenberg JR, Amjad AM, Breeze P, Conway BA, Farmer SF. A framework for the analysis of mixed time series/point process data—theory and application to the study of physiological tremor, single motor unit discharges and electromyograms. Prog Biophys Mol Biol 1995;64(2–3):237–78.
Halliday DM, Conway BA, Farmer SF, Rosenberg JR. Using electroencephalography to study functional coupling between cortical activity and electromyograms during voluntary contractions in humans. Neurosci Lett 1998;241:5–8.
Halliday DM, Conway BA, Christensen LOD, Hansen NL, Petersen NP. Functional coupling of motor units is modulated during walking in human subjects. J Neurophysiol 2003;89:960–8.
Hansen NL, Hansen S, Christensen LOD, Petersen NT, Nielsen JB. Synchronization of lower limb motor unit activity during walking in human subjects. J Neurophysiol 2001;86(3):1266–76.
Hansen NL, Conway BA, Halliday DM, Hansen S, Pyndt HS, Biering-Soresnsen F. Reduction of common synaptic drive to ankle dorsiflexor motoneurones during walking in patients with spinal cord lesion. J Neurophysiol 2005;94:934–42.
Haykin S. Adaptive filter theory. Fourth edition New Jersey: Prentice Hall; 2004.
Kandel ER, Schwartz JH, Jessell TM. Principles of Neural Science. fourth edition Ohio: McGraw-Hill; 2000.
Lachaux J-P, Lutz A, Rudrauf D, Cosmelli D, Quyen MLV, Martinerie J. Estimating the time-course of coherence between single-trial brain signals: an introduction to wavelet coherence. Neurophysiol Clin 2002;32:157–74.
Murray MP, Mollinger LA, Gardner GM, Sepic SB. Kinematic and EMG patterns during slow, free, and fast walking. J Orthop Res 1984;2(3):272–80.
Nielsen J, Kagamihara Y. Synchronization of human leg motor units during co-contraction in man. Exp Brain Res 1994;102:84–94.
Nielsen JB, Conway BA, Halliday DM, Perreault M-C, Hultborn H. Organization of common synaptic drive to motoneurones during fictive locomotion in the spinal cat. J Neurophysiol 2005;569:291–304.
Percival DB, Walden AT. Spectral analysis for physical applications: multitaper and convential univariate techniques. Cambridge: Cambridge University Press; 1998.

Percival DB, Walden AT. Wavelet methods for time series analysis. Cambridge: Cambridge University Press; 2000.
Thomson DJ, Chave AD. Jackknifed error estimates for spectra, coherences, and transfer functions. In: Haykin S, editor. Advances in spectrum analysis and array processing, 1. New Jersey: Prentice Hall; 1991. p. 58–113.
Thomson DJ. Spectrum estimation and harmonic analysis. Proc IEEE 1982;70(9): 1055–96.
Thomson DJ. Multitaper analysis of nonstationary and nonlinear time series data. In: Fitzgerald WJ, Smith RL, Walden AT, Young P, editors. Nonlinear and nonstationary signal processing. Cambridge: Cambridge University Press; 2000.